Macromolecules
ARTICLE

Macromolecules **2010**, *43*, 3757–3763 **3757**
DOI: 10.1021/ma902817g

Calorimetric Characterization of the Heterogeneities Produced by the Radiation-Induced Cross-Linking Polymerization of Aromatic Diacrylates

Mickael Krzeminski,[†] Michael Molinari,[‡] Michel Troyon,[‡] and Xavier Coqueret*,[†]

[†]*Université de Reims Champagne-Ardenne, Institut de Chimie Moléculaire de Reims CNRS UMR 6229, Moulin de la Housse, BP 1039, 51687 Reims Cedex 2, France, and* [‡]*Laboratoire de Microscopies et d'Etude de Nanostructures, LMEN EA3799, 21 rue Clément Ader, 51685 Reims Cedex 2, France*

Received December 22, 2009; Revised Manuscript Received February 21, 2010

ABSTRACT: The structural heterogeneities in networks produced by UV- and by electron beam-initiated polymerization of aromatic diacrylates were unambiguously revealed by AFM imaging and studied by means of temperature-modulated differential scanning calorimetry. Two main second-order thermodynamic transitions were observed during the analysis of diacrylate networks exhibiting a fractional degree of conversion ranging from 0.1 to 0.8. The bimodal distribution of transition temperatures observed as fused peaks in the diagrams representing the differential quantity associated with the reversing heat capacity, $dC_{p,rev}/dT$, was satisfactorily resolved by a two-component numerical fitting method allowing a quantitative exploitation of the data in terms of Gaussian contributions with particular central relaxation temperature and peak width affected by the gradual polymerization of the sample. The dual relaxation phenomenon was assigned to a biphasic-like structure consisting of clusters with a high cross-link density formed in continuous domain of lower monomer conversion. The evolution of the calorimetric data in the samples affords detailed information on the gradual formation of the network, with the initial broadening and final narrowing of the transition peak at high temperature related to the densely cross-linked clusters, whereas the low-temperature transition vanishes in intensity with an increasing broadening of the associated transition range. The analyses carried out in this work did not point out any influence of the UV- or EB-induced initiation mechanism of the time scale and thermal conditions of the polymerization process on the calorimetric features of the observed heterogeneities.

Introduction

The radiation-initiated cross-linking polymerization of liquid formulations of multifunctional monomers receive increasing attention because of its quite unique reactivity for triggering the formation of densely cross-linked networks. The method yields materials exhibiting mechanical and functional properties exploited in a number of applications,[1] particularly in the printing and coating industries.

However, free radical cross-linking polymerization is subject to complex chain growth mechanism and chain kinetics.[2,3] It is considered by several authors to produce networks very heterogeneous in structure and possibly in composition.[4,5] Localized autoacceleration of polymerization in the early stages of the reaction is commonly invoked as a consequence of very fast intramolecular cyclization[3,5] together with intermolecular cross-linking. These combined events can form cross-linked clusters swollen by monomers that are sometimes named microgels in reference to the intermediate stage of vinyl ester−styrene networks upon formation. As the polymerization proceeds, the number of microgels is believed to increase. The continuation of polymerization inside the clusters induces their gradual vitrification, whereas the polymerization in interstitial domains finally achieves the interconnection of percolating vitreous clusters. Various questions arise about the actual scenario describing the build-up of the final monolithic material.

The existence of heterogeneities is believed to exert a strong influence on the optical, mechanical, and permeation properties of the resulting materials. A notable feature of the densely cross-linked systems produced by fast polymerization of multifunctional monomers is their brittleness[6] that limits their use in various domains where a high level of mechanical resistance is required. This type of mechanical limitation is particularly acute for UV-curable coatings[7] and adhesives,[8] as well as for the emerging sector of radiation-curable structural composites.[9,10]

Experimental evidence of the presence of structural microheterogeneities has been pointed out through a variety of physical methods including thermomechanical measurements,[11−13] dielectric analyses,[14,15] or spectroscopic techniques such as solid state NMR.[16−18] Nevertheless, only imaging techniques can provide unambiguous evidence of spatial heterogeneity[19] with indications on the typical dimension and morphology of the constituting domains.

Preliminary experiments using atomic force microscopy (AFM) in the tapping mode were conducted to visualize simultaneously the local topography together with the variations of cross-linking density. The picture of Figure 1 shows both the height and the phase images of a film made of bis-phenol A epoxy diacrylate (EPAC) cured under ultraviolet radiation with a low amount of photoinitiator (0.1 wt %) to a conversion level of $\pi = 0.41$. The topographical image shows a very flat sample with a rms roughness of 0.2 nm, whereas the phase contrast image highlights a more complex and heterogeneous structure. The apparent morphology is composed of very stiff domains corresponding to the lower phase values, whereas the darker zones correspond to much more compliant material. Stiff domains can be reasonably associated with the presence of clusters, originating from the initial microgels. Those clusters exhibit a densely cross-linked structure that contrasts with the softer interstitial zones that likely

*Corresponding author. Tel/Fax: 33 3 26 91 33 38. E-mail: xavier.coqueret@univ-reims.fr.

Published on Web 03/23/2010

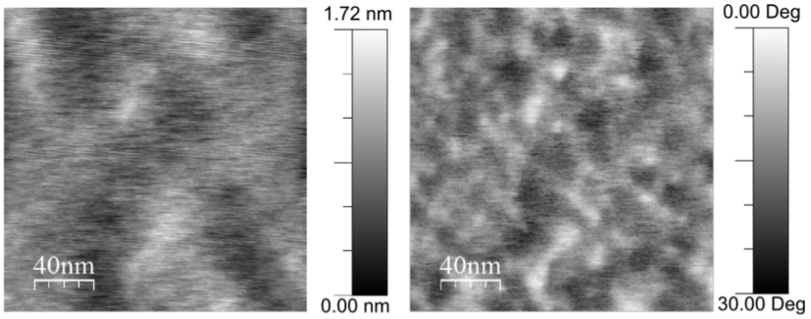

Figure 1. Height (left) and phase contrast (right) AFM images recorded in tapping mode of partially UV-cured ($\pi = 0.41$) EPAC network.

Scheme 1. Structure of the Studied Diacrylate Monomers

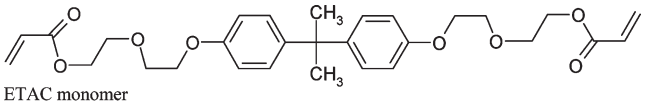
ETAC monomer

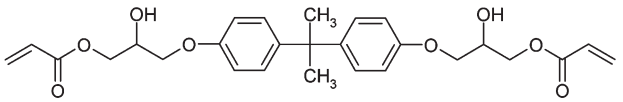
EPAC monomer

correspond to the loosely cross-linked and swollen matrix. This type of image supporting without ambiguity the existence of dense nodules with a mean diameter of about 15 nm casts doubts on a number of common models interpreting the progress of polymerization by the kinetic laws applicable to homogeneous media and describing the structure of the final material in terms of homogeneous network morphology. Hence, the description and understanding of the structure−property relations in multiacrylate networks by taking into account their microheterogeneity is important from both fundamental and practical viewpoints.

In this article, we report on the calorimetric properties of networks obtained by radiation-initiated polymerization of two diacrylates derived from bis-phenol A (BPA), an ethoxylated BPA diacrylate named ETAC and an BPA epoxy diacrylate named EPAC, that exhibit distinct structures, essentially because of the presence of possibility of intermolecular H-bonding in EPAC (Scheme 1). Hence, different physical properties in the liquid monomer state as well as in the cured state are expected. The first experiments conducted by using the temperature-modulated mode of differential scanning calorimetry (TMDSC) allowed us to record thermograms with superior relevance for a detailed quantification of the thermal parameters characterizing the analyzed networks. We have examined comparatively the influence of the mechanism of initiation by studying two series of samples, prepared either by photochemical activation via a free-radical initiator or by application of an ionizing radiation with a 10 MeV electron beam.

Experimental Section

Material and Polymerization Procedure. Ethoxylated bisphenol A diacrylate (ETAC) from Sartomer (reference SR601E) and bis-phenol A epoxy diacrylate (EPAC) from Cytec (reference Ebecryl 600) were used as received, without diluent.

We achieved photopolymerization was achieved under 365 nm UV irradiation (Philips TL08, 7 mW·cm^{-2}) by exposing the liquid monomer mixed with a limited amount (0.1 wt % for samples with conversion up to 0,55) of 2-hydroxy-2-methylpropiophenone (Additol HDMAP, Cytec). The DSC pans containing the formulations (thickness from 1.5 to 1.6 mm) were covered with 100 μm thick PET film before curing. Curing temperature (set between 25 and 125 °C, Linkam hot stage) and exposure duration (10 to 60 min) were varied for obtaining acrylate conversion levels ranging from 0.1 to 0.6.

For obtaining samples with higher conversion ($0.6 < \pi < 0.75$), the amount of photoinitiator was raised to 2 wt %. Under the conditions of our experiments (sample thickness, irradiation spectrum of the source, photoinitiator absorption), it was found that the mean absorbance of the sample was ~0.2. Consequently, the internal screening effect is very limited, allowing almost uniform polymerization in the depth of the samples. IR measurements did not reveal any significant difference of monomer conversion between the two sides of the exposed samples.

For samples cured by electron beam irradiation, no photoinitiator was used. Small vials of diameter not exceeding 1 cm were filled with a controlled amount of diacrylate monomer (6 to 7 g) and submitted to EB irradiation at room temperature. The 10 MeV pulsed electron beam of the CIRCE II generator (Linac Technologies) ensured homogeneous energy deposition through the entire samples. The applied doses were ranging from 5 to 160 kGy applied by increment never exceeding 25 kGy so as to limit excessive temperature rise within the samples.

Conversion Monitoring. Conversion of studied samples was checked using Fourier transform infrared spectroscopy (FTIR). Spectra were recorded using a Bruker alpha spectrophotometer on potassium bromide pellets including 5 wt % of the powdered sample. The decrease in absorbance at 810 cm^{-1} (−CH=CH$_2$ out of plan deformation) was measured taking into account that the invariant band centered at the reference wavenumber 830 cm^{-1} A^t_{830} (aromatic −CH= deformation) has a contribution to the absorbance A^t_{810} measured at 810 cm^{-1} amounting to 16% of A^t_{830}. The conversion was thus calculated using the following equation

$$\pi = 1 - \frac{A^t_{810} - 0.16A^t_{830}}{A^0_{810} - 0.16A^0_{830}} \quad (1)$$

AFM Observation. AFM experiments were conducted on 20 μm thick films polymerized under a nitrogen atmosphere so as to avoid surface inhibition by oxygen. Images were acquired in the tapping mode using an AFM apparatus Dimension from Veeco. In particular, we used a silicon tip with a nominal resonance frequency of 320 kHz and a nominal spring constant of 42 N·m^{-1}.

TMDSC Analysis. A representative fraction of the cured material (5−8 mg) was cut and placed into a hermetic DSC pan. TMDSC measurements were carried on a Q100 DSC apparatus from TA Instruments upgraded with the temperature-modulation package. TMDSC scans were recorded on cooling mode with nitrogen as purge gas. The pristine sample was heated over its glass transition and kept at the starting temperature for 5 min before beginning the modulated cooling ramp down to the vitreous state. Because of the very broad variation of glass-transition temperature over the conversion range, the starting temperature was chosen to be 70 °C above expected glass-transition temperature to limit thermal aging.

The thermograms were processed by the Origin v8.0 software to obtain the differential quantity $dC_{p,rev}/dT$ and to resolve the resulting bimodal curves by a two-component Gaussian fit.

Results and Discussion

Temperature-Modulated DSC for Multicomponent and Heterogeneous Systems. One of the most important features of temperature-modulated DSC (TMDSC) compared with conventional calorimetric analysis is the separation into the reversing and nonreversing components of the global heat exchanges,[20] particularly when perturbing phenomena blur the signals of interest and impede the analysis of the glass transition. The glass transition and the morphology of multicomponent polymers has been studied by using the derivative of the reversing heat capacity ($C_{p,\mathrm{rev}}$).[21] At the same period, it was established on a theoretical background that the derivative of the reversing heat capacity of a pure polymer has a Gaussian form.[22] Song et al. have successfully studied the glass transition and morphology of multicomponent polymer materials and were able to distinguish different glass-transition temperatures distant by a 15 °C interval. A similar approach was also applied to study the microheterogeneity of an urethane vinyl ester resin cross-linked with styrene.[23] The treatment of calorimetric data revealed the asymmetry of the glass-transition relaxation peak of fully cured samples. The dual relaxation phenomenon was attributed to a microphase separation with polystyrene-rich zones and vinyl-ester-rich zones.

We therefore considered the TMDSC technique as a potential method for probing the heterogeneous structure of multiacrylate networks and for exploring the gradual build-up of the network upon UV- or EB-initiated polymerization.

Experimental Aspects. A recurrent issue in the thermal analysis of partially cured materials with potential sensitivity to heat activation is to warrant the absence of any irreversible chemical or physical change during the probing experiment or at least to minimize the resulting evolution at a controlled level. TMDSC is not exempt from that risk of sample evolution during analysis.

A first question is related to possible increase in monomer conversion induced by the thermal treatment. The scanning experiments being conducted in the cooling mode, the sample is necessarily heated over its glass-transition temperature before data recording, with possible undesired evolution. To evaluate the importance of the possible chemical changes, DSC pans were submitted to repeated heating and cooling scans and checked for monomer conversion by FTIR spectroscopy. The results of Figure 2 give the conversion data recorded for EPAC networks before and after the TMDSC runs. Samples 1, 2, and 4 have been submitted to one run, whereas three runs were carried out on sample 3. After one run applied to a sample of very low initial conversion (π = 0.11), the new measured π value is 0.15, corresponding to a rather high relative increase (about +36% variation in sample 1) but still limited in absolute variation of π ($\Delta\pi$ = 0.04). In the other samples of higher initial conversion, the observed variations are much more limited after a single scan ($\Delta\pi \cong 0.02$). Repeating the heating and cooling cycles has a slightly higher impact on sample conversion. In sample 3, for example, the absolute variation of π ($\Delta\pi$ = 0.04) is determined after subjecting the sample to three heating ramps a sample of initial conversion π = 0.41. Considering the experimental error inherent to FTIR technique and spectrum recording on pellets, we can conclude that only limited change on ETAC and EPAC networks occurs during heating phase over sample glass transition or during TMDSC run and consequently that analyses carried out are representative of network obtained after polymerization. These observations are consistent with previous results,[24] which showed on similar chemistry that thermal aging would imply significant conversion increase on a time scale of several dozen hours. On the time scale of our analyses, postpolymerization is a very limited perturbing phenomenon.

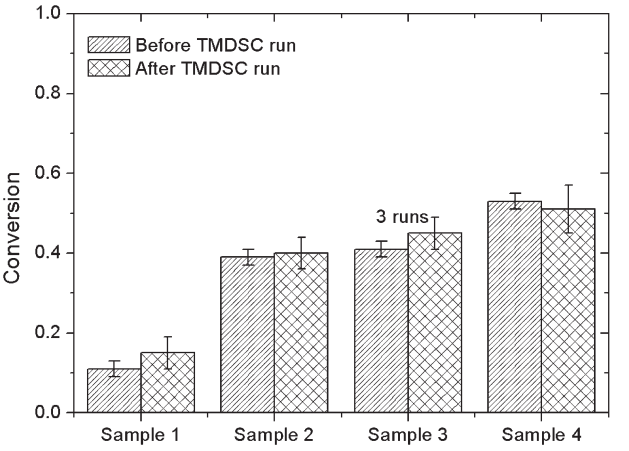

Figure 2. Effect of heating ramps on the monomer conversion determined by FTIR analysis in EPAC network samples UV-polymerized (7 mW·cm^{-2}, 0.1 wt % of photoinitiator) to various conversion levels and submitted to TMDSC.

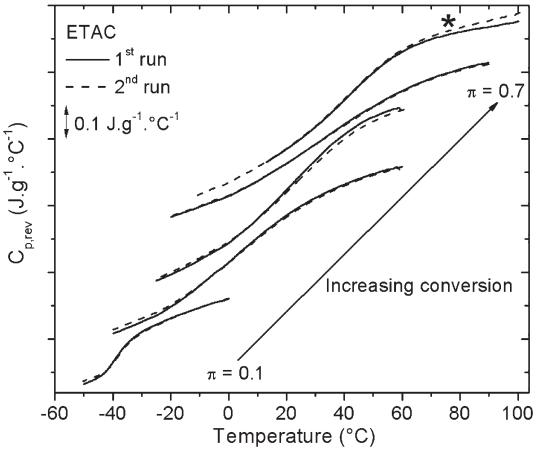

Figure 3. Comparison of the TMDSC thermograms recorded during the first and second cooling ramp for ETAC networks EB-cured to various conversion levels (dose ranging from 5 to 80 kGy for the curve marked with a star).

In chemically stable systems but including constituents of poor mutual compatibility, the difference between the two consecutively recorded thermograms can indeed be interpreted by the occurrence or progress of phase separation.[25] A series of analyses was therefore conducted to evaluate further the possible changes in the calorimetric behavior of the sample by repeating the heating−cooling scans of a typical TMDSC analysis. The plots of Figure 3 show the $C_{p,\mathrm{rev}}$ curves obtained on EB-cured ETAC networks covering a large range of monomer conversion, each sample being submitted to two consecutive TMDSC runs. The curves obtained during the first and the second runs are very similar, and only a minor shift of the baseline can be observed before or after glass transition. We therefore concluded from these observations that no significant change in the constitution of the analyzed material was occurring during the first two TMDSC runs. The calorimetric data determined for each sample were therefore assigned to the structural features of the pristine sample as obtained after radiation-curing.

Background of the Analysis. The singularities of the curves representing the variation of reversing heat capacity appear clearly in the graphical representations as those of Figure 3. However, the determination of the central value of the second-order transition as well as the width of the corresponding temperature range are not precisely assessed.

More useful information can be obtained from the original data by plotting the derivative of reversing heat capacity with respect to temperature $dC_{p,rev}/dT$ (Figure 4). The derivative of the reversing heat capacity measured for the unreacted monomer shows a narrow single Gaussian peak. For UV-cured EPAC networks with conversion degrees π ranging from 0.12 to 0.76, the signal amplitude decreases as the degrees of freedom for the system decrease, when simultaneously it also tends to gradually broaden, with the development of a shoulder. Two distinct situations can be observed depending on the level conversion, lower or higher than a critical value roughly defined as $\pi = 0.5$. Below this conversion, the shoulder appears at a temperature above the one corresponding to the maximum of the reversing heat capacity curve, whereas for higher conversions, it occurs at lower temperature. Considering that at low conversion, the domains can be initially produced in the form of isolated microgels showing higher conversion level than the surrounding medium, hence exhibiting a higher glass transition, the main relaxation peak at low temperature and the shoulder developing at higher temperature can be assigned accordingly. At higher conversion, the situation is reversed with a higher fraction of domains vitreous at room temperature, the low temperature shoulder being assigned to the interstitial loosely cross-linked domains.

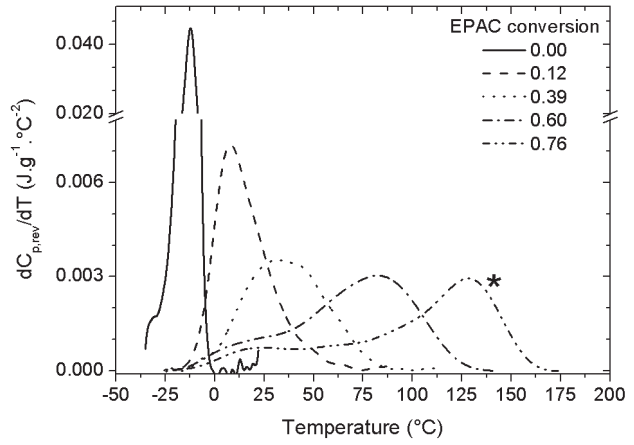

Figure 4. Curves representing the variations of the derivative of the reversing heat capacity signals $dC_{p,rev}/dT$ for EPAC networks UV-polymerized to various conversion levels (7 mW·cm^{-2}, photoinitiator content: 0.1 wt %, 2 wt % for the curve marked with a star).

The thermograms can be further exploited to compute the differential quantity $dC_{p,rev}/dT$ associated with the reversing heat capacity signal. In an attempt to characterize quantitatively the relaxations of the different domains in the networks, we have chosen to fit the experimental values of $dC_{p,rev}/dT$ with a sum of two Gaussian curves[26] as described by eq 2

$$\frac{dC_{p,\mathrm{rev}}}{dT} = \sum_{i=1}^{2} \frac{\Delta C_{p,i}}{\Delta T_{g,i}(\pi/2)} \exp\left(-\frac{2(T - T_{g,i})^2}{\Delta T_{g,i}^2}\right) \qquad (2)$$

where $\Delta C_{p,i}$ is the increment of heat capacity of the relaxing domain i, $\Delta T_{g,i}$ is the half width, and $T_{g,i}$ is the center of the peak corresponding to its glass-transition temperature. Subscript 1 refers to the transition occurring at lower temperature (monomer rich domains and then loosely cross-linked domains), and subscript 2 refers to the transition occurring at higher temperature (i.e., the highly cross-linked microdomains).

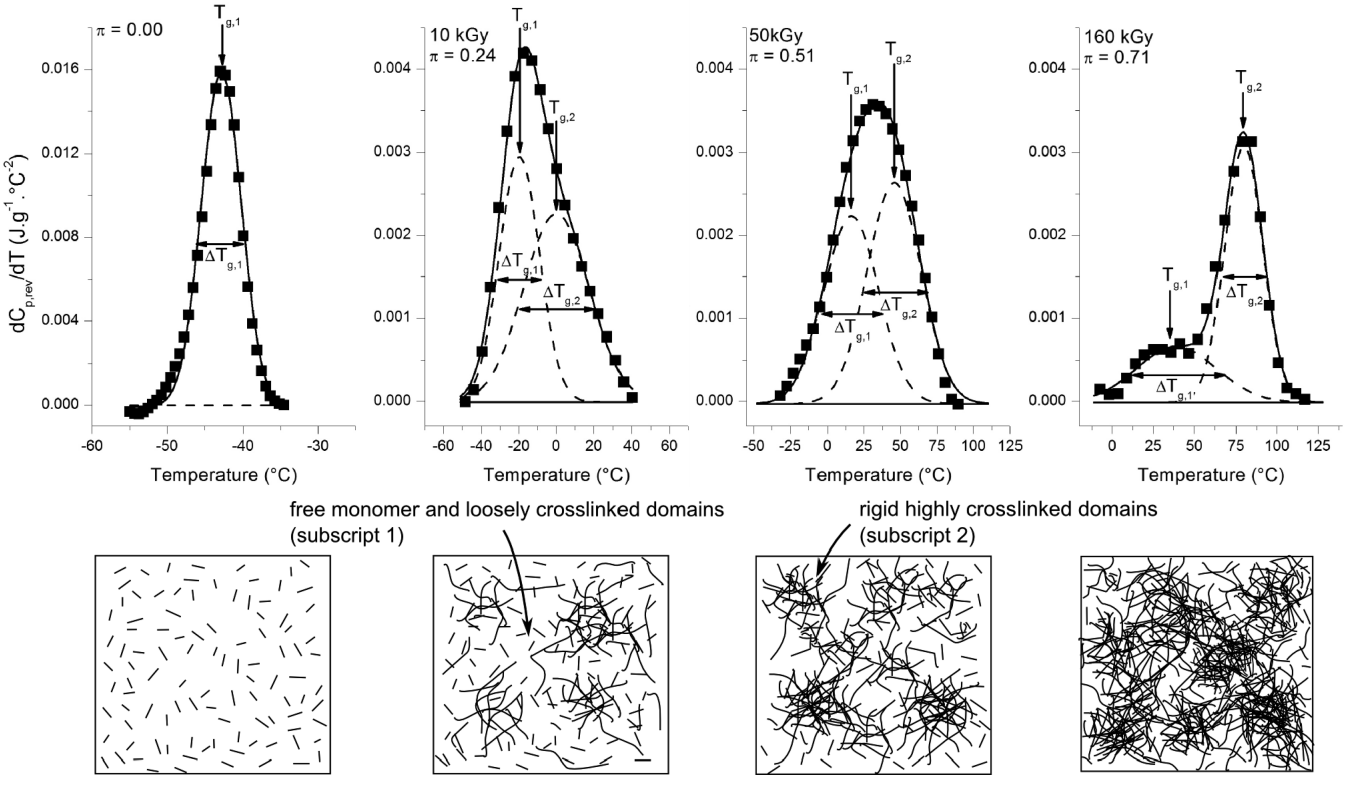

Figure 5. Examples of peak resolutions of the $dC_{p,rev}/dT$ curves for a set of EB-cured ETAC networks (dose and conversion shown on the graphs) and corresponding schematic representation of heterogeneity.

Therefore, the calorimetric behavior of each network possessing a given conversion degree is depicted by two transitions characterized by a set of two parameters of interest, namely, the central value $T_{g,i}$ of the relaxation phenomenon and $\Delta T_{g,i}$ the width at half-height of the relaxation peak.

This is illustrated in Figure 5, representing four examples of peak resolutions for the $dC_{p,rev}/dT$ curves obtained from EB-cured ETAC networks. The reported results correspond to solutions combining satisfactory mathematical relevancy and acceptable physical meaning, particularly in terms of continuity for the set of parameters. The observed standard errors on fitted parameters were typically ranging between 1 and 3%. The corresponding error bars were not added to data points for the sake of clarity. In a limited number of cases, some nonreproducible events in the heat flux resulted in an additional maximum of weak intensity in the $dC_{p,rev}/dT$ curves. The associated area was shown to contribute to $< 4\%$ in surface fraction relative the two main distributions. Those minor events were attributed to experimental artifacts or perturbations, and consequently not considered for the discussion.

Analysis of Glass-Transition Temperatures. The plots of Figure 6 show the variations of the central values $T_{g,i}$ obtained after best fitting treatments applied to the data obtained from samples of ETAC (Figure 6a) and EPAC (Figure 6b) networks polymerized to various degrees of conversion (π) by UV or electron beam initiation. It can be noticed that even with π values as low as 0.1, two curves are needed to describe satisfactorily the observed sample response, which means that heterogeneities interpreted in terms of microgels appear very soon, even when the polymerization media is still fluid with sufficient mobility to achieve cross-linking between two isolated growing chains. The $T_{g,i}$ values exhibit a monotone growth over the explored conversion range as a logical consequence of increasing cross-link density with conversion. In particular, the two $T_{g,i}$ master curves plotted for the low and high temperature components can be both fitted with the Havlicek and Dusek[27] empirical relation (eq 3) linking glass transition and conversion

$$\frac{1}{T_{g,i}} = \frac{1-\pi}{T^0_{g,i}} + \frac{\pi}{T^\infty_{g,i}} + C\pi(1-\pi) \qquad (3)$$

where $T^0_{g,i}$ is the glass-transition temperature for $\pi = 0$, $T^\infty_{g,i}$ is the glass-transition temperature at full conversion ($\pi \approx 1$), and C is a numerical adjustment parameter.

For a given conversion, $T_{g,i}$ is higher for the EPAC network than for the ETAC network. This difference is essentially explained by the distinct linkers connecting the acrylate function to the central bis-phenol A moieties in the network precursors. Whereas ETAC monomer possesses a flexible ethoxy linker, the presence of hydroxyl functions in the oxypropylidene segment of EPAC allows for the formation of hydrogen bonds resulting in additional mobility restriction by intermolecular associations.

It is also particularly interesting to notice that no significant distinction can be made between samples polymerized under ultraviolet or electron beam irradiation. For a given conversion, UV- and EB-cured samples present very similar $T_{g,i}$ values. This observation points out the minor influence of the initiation mode and curing conditions on the ultimate thermal properties of the formed networks. Indeed, whereas samples polymerized under UV lamps undergo slow and almost isothermal curing by means of a temperature-regulated hot stage, EB-cured samples were polymerized according to very anisothermal conditions because the material's temperature is governed in this case by electron energy deposition and related polymerization exothermicity.[28]

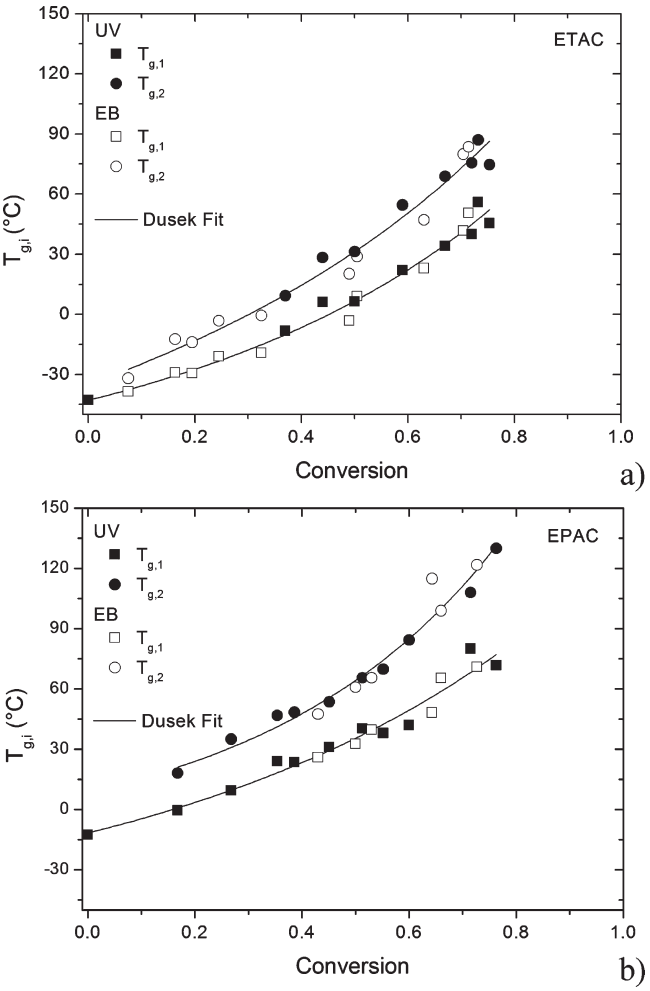

Figure 6. Plots of the variations of $T_{g,i}$ and of the corresponding fit curves for (a) ETAC and (b) EPAC networks polymerized under radiation (UV or electron beam EB) to various conversion levels.

The issues related to the influence of initiation mechanism and time scale of the cross-linking polymerization are currently under investigation and will not be discussed in this article focused on the physical characteristics of the networks.

Network Build-up and Morphology. The data discussed in the previous section on the properties of the distinct domains within the heterogeneous networks were much in the line of the conversion dependence of T_g, as a central property. A deeper analysis can be achieved by examining the width of each glass transition. The variations of the corresponding $\Delta T_{g,2}$ and $\Delta T_{g,1}$ values plotted in Figures 7 a,b and 8a,b as a function of monomer conversion do not follow the same profile, revealing contrasting evolutions in the two types of domains. The width of the low-temperature transition $\Delta T_{g,1}$ follows a monotonous increase over the explored conversion range, whereas $\Delta T_{g,2}$ increases at first until monomer conversion reaches the critical value π close to 0.5, and then $\Delta T_{g,2}$ decreases when the conversion approaches 0.8.

The $\Delta T_{g,2}$ values are assigned to the domains initially generated as microgels in the liquid monomer, which will undergo vitrification and eventually form by aggregation the highly cross-linked monolithic phase of the diacrylate materials. The data of Figure 7 a,b show that $\Delta T_{g,2}$ increases until a critical domain in the intermediate conversion range

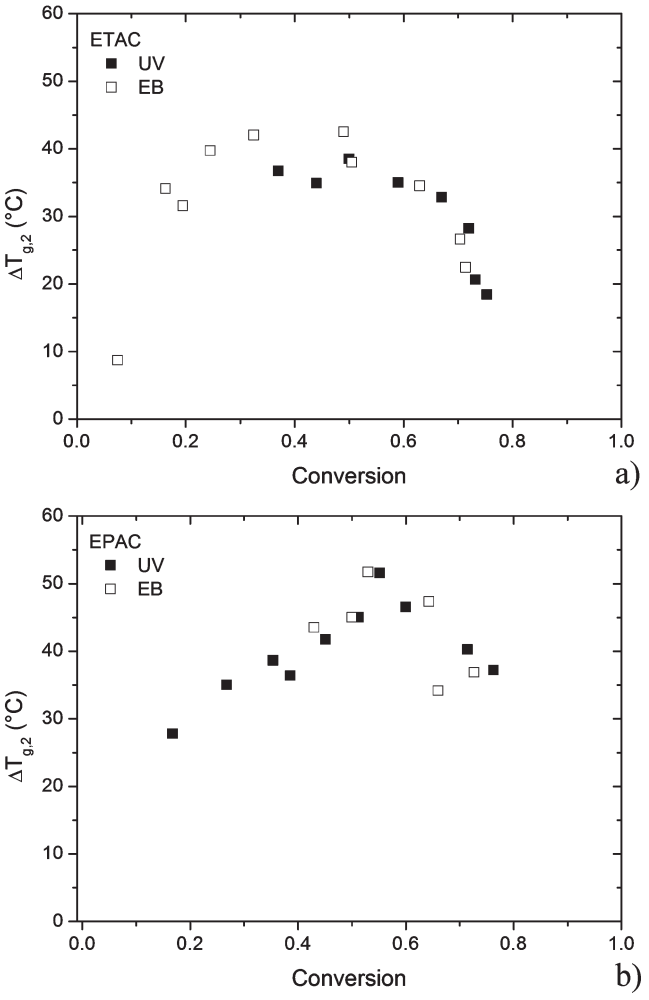

Figure 7. Plots of the variations of $\Delta T_{g,2}$ for (a) ETAC and (b) EPAC networks polymerized under radiation (UV or electron beam EB) to various conversion levels.

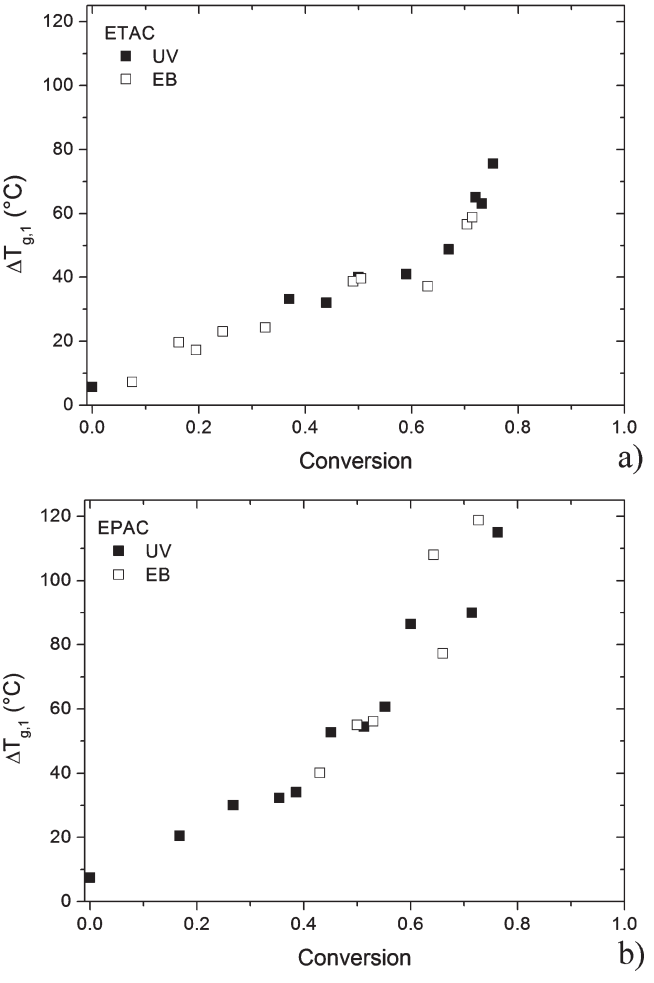

Figure 8. Plots of the variations of $\Delta T_{g,1}$ for (a) ETAC and (b) EPAC networks polymerized under radiation (UV or electron beam EB) to various conversion levels.

($0.3 < \pi < 0.6$) and then decreases when the conversion is further increased up to values approaching 0.8. This general behavior is qualitatively similar for the two diacrylates. For the ETAC networks, the highest values $(\Delta T_{g,2})_{max}$ close to 40 °C are observed for a conversion domain ranging from 0.3 to 0.5, whereas the maximum seems to reach a little higher value ($45 < (\Delta T_{g,2})_{max} < 50$) observed at a slightly higher conversion ($\pi = 0.55$) for the EPAC networks.

The $\Delta T_{g,1}$ values of a given monomer are assigned to the initially continuous domains with low monomer conversion that are surrounding the nucleated microgels. The latter increases in numbers and possibly in size upon continuation of the radiation-induced initiation, thus reducing the volume fraction of the softer material that is finally believed to be restricted to interstitial zones. The variations of $\Delta T_{g,1}$ as a function of conversion shown in Figure 8a,b show a monotonous increase over the whole range of conversion that is expanding from 10 to 80 °C for ETAC and to 120 °C for EPAC networks. This can be interpreted by polymerization taking place in various constrained environments, generating a variety of situations for completing the polymerization.

This strongly contrasts with the polymerization of the high T_g domains, which seems to bring the clusters generated locally and later percolated toward a well-defined state with a reduced distribution of relaxation temperatures.

By comparing the data obtained from UV- and electron-beam-polymerized samples, it clearly appears, as previously observed for the evolution of $T_{g,i}$ values, that no significant differences in $\Delta T_{g,i}$ results, for the systems under study, from initiation mechanism or from the curing conditions.

Further work is currently in progress to investigate the features of microheterogeneous networks produced by radiation-initiated polymerization of aromatic diacrylates further. In particular, the combination of conventional analytical methods (DMA, pycnometry) and advanced techniques (AFM, NMR relaxation experiments) applied to samples covering a broad range of monomer conversion provide various pictures, making it possible to draw a realistic scenario of the cross-linking polymerization.

Conclusions

We have shown that TMDSC allows the fine thermal characterization of radiation-cured diacrylate networks by revealing distinct glass-transition temperatures. On the basis of previous observations done on similar samples and further supported by AFM images revealing the presence of nanoscale heterogeneities with constrating elastic response in the tapping mode, a two-component model was applied to the differential quantity $dC_{p,rev}/dT$. The treatment allows determining the calorimetric features of the two domains constituting the analyzed samples. A series of samples covering a broad range of monomer conversion were analyzed accordingly, showing that the domains exhibiting the high transition temperature undergo an evolution toward a well-defined state with a narrowing distribution of relaxation

temperatures at the higher conversion values, whereas the low-temperature relaxation is continuously extending over a wider domain of temperatures.

The results were interpreted on the basis of AFM images showing the formation of rigid clusters initially formed as microgels in the early stages of the polymerization and further evolving with the increase in cross-link density. The evolution of these microgels growing in number and in size strongly influences polymerization by creating interstitial domains with lower cross-link density but a larger number of defects. Finally, no significant influence of initiation mechanism, polymerization time scale, or curing temperature conditions was observed on the calorimetric features of the diacrylate networks. This peculiarity is probably the result of the very fast and localized cross-linking polymerization, which reduces the influence of the initiation mechanism and of the overall polymerization kinetics.

Acknowledgment. We express our gratitude to Dr. B. Defoort and Dr. G. Larnac (Astrium Space Transportation) for their continuous encouragements and aid to our studies on radiation-induced polymerization. Financial support by Conseil Regional Champagne Ardenne, MENESR and EU-FEDER Programme (CPER Project PlAneT) and by the EADS Foundation is gratefully acknowledged.

References and Notes

(1) Burchill, P. J.; Pearce P. J. In *Polymeric Materials Encyclopedia*; Salamone, J. C., Ed.; CRC Press: New York, 1996; p 2204.
(2) Itaru, M.; Kazuyuki, H. *J. Macromol. Sci., Rev. Macromol. Chem. Phys.* **1987**, *C27*, 91–169.
(3) Dusek, K.; Galina, H.; Mikes, J. *Polym. Bull.* **1980**, *3*, 19–25.
(4) Bowman, C. N.; Kloxin, C. J. *AIChE J.* **2008**, *54*, 2775–2795.
(5) Wen, M.; Scriven, L. E.; McCormick, A. V. *Macromolecules* **2003**, *36*, 4140–4150.
(6) Rey, L.; Duchet, J.; Galy, J.; Sautereau, H.; Vouagner, D.; Carrion, L. *Polymer* **2002**, *43*, 4375–4384.
(7) Chen, Z.; Chisholm, B.; Kim, J.; Stafslien, S.; Wagner, R.; Patel, S.; Daniels, J.; Vander Wal, L.; Li, J.; Ward, K.; Callow, M.; Thompson, S.; Siripirom, C. *Polym. Int.* **2008**, *57*, 879–886.
(8) Goss, B. *Int. J. Adhes. Adhes.* **2002**, *22*, 405–408.
(9) Burchill, P. J.; Kootsookos, A.; Lau, M. *J. Mater. Sci.* **2001**, *36*, 4239–4247.
(10) Coqueret, X.; Krzeminski, M.; Ponsaud, P.; Defoort, B. *Radiat. Phys. Chem.* **2009**, *78*, 557–561.
(11) Kannurpatti, A. R.; Anseth, J. W.; Bowman, C. N. *Polymer* **1998**, *39*, 2507–2513.
(12) Kannurpatti, A. R.; Anderson, K. J.; Anseth, J. W.; Bowman, C. N. *J. Polym. Sci., Part B: Polym. Phys.* **1997**, *35*, 2297–2307.
(13) Guo, Z.; Browne, E.; Compton, J.; Sautereau, H.; Kranbuehl, D. *J. Non-Cryst. Solids* **2006**, *352*, 5025–5028.
(14) Kannurpatti, A.; Bowman, C. *Macromolecules* **1998**, *31*, 3311–3316.
(15) Guo, Z.; Sautereau, H.; Kranbuehl, D. E. *Macromolecules* **2005**, *38*, 7992–7999.
(16) Litvinov, V.; Dias, A. *Macromolecules* **2001**, *34*, 4051–4060.
(17) Litvinov, V. M.; Dias, A. A. *Macromol. Symp.* **2005**, *230*, 20–25.
(18) Jager, W.; Lungu, A.; Chen, D.; Neckers, D. *Macromolecules* **1997**, *30*, 780–791.
(19) Anseth, K. S.; Bowman, C. N. *J. Polym. Sci, Part B: Polym. Phys.* **1995**, *33*, 1769–1780.
(20) Simon, S. L. *Thermochim. Acta* **2001**, *374*, 55–71.
(21) Hourston, D. J.; Song, M.; Hammiche, A.; Pollock, H. M.; Reading, M. *Polymer* **1997**, *38*, 1–7.
(22) Song, M.; Hourston, D. J.; Schafer, F. U.; Pollock, H. M.; Hammiche, A. *Thermochim. Acta* **1997**, *304/305*, 335–346.
(23) Zhang, J.; Richardson, M. O. W. *Polymer* **2000**, *41*, 6843–6849.
(24) Defoort, B.; Lopitaux, G.; Dupillier, J. M.; Larnac, G.; Coqueret, X. *Macromol. Chem. Phys.* **2001**, *202*, 3149–3156.
(25) Stubbs, J. M.; Sundberg, D. C. *J. Polym. Sci., Part B: Polym. Phys.* **2005**, *43*, 2790–2806.
(26) Hourston, D. J.; Song, M.; Schafer, F. U.; Pollock, H. M.; Hammiche, A. *Polymer* **1999**, *40*, 4769–4775.
(27) Havlicek, I.; Dusek, K. In *Crosslinked Epoxies*; Sedlacek, B., Kahovec, J., Eds.; Walter de Gruyter & Co.: Berlin, 1987; p 417.
(28) Defoort, B.; Defoort, D.; Coqueret, X. *Macromol. Theor. Simul.* **2000**, *9*, 725–734.